

# Structural and magnetic properties of spin chain compounds $\text{Ca}_3\text{Co}_{2-x}\text{Fe}_x\text{O}_6$

A. Jain, Sher Singh, and S. M. Yusuf\*

Solid State Physics Division, Bhabha Atomic Research Centre, Mumbai 400085, India

(Received 31 July 2006; revised manuscript received 5 October 2006; published 17 November 2006)

We report the structural and magnetic properties of quasi-one-dimensional (1D) spin chain compounds  $\text{Ca}_3\text{Co}_{2-x}\text{Fe}_x\text{O}_6$  ( $x=0, 0.1, 0.2,$  and  $0.4$ ). Simultaneous Rietveld refinement of powder neutron and x-ray diffraction patterns at room temperature confirmed the single-phase formation for all the samples in the rhombohedral structure with space group  $R\bar{3}c$ . Rietveld refinement and Mössbauer study confirmed that  $\text{Fe}^{3+}$  ion was doped at trigonal prism site,  $6a$  (0, 0, 1/4) of Co. Decrease of intrachain positive exchange constant  $J$  and increase of interchain negative exchange constant  $J'$  with iron substitution result in deviation from “1D character” in these spin chain compounds. Deviation from the  $H^{-3/2}$  dependence of magnetization-approach to its saturation value for higher iron concentration ( $x=0.4$ ) further supports this observation. The observed results have been ascribed to a breaking of the ferromagnetically ordered linear spin chains along the crystallographic  $c$  axis with iron doping and strengthening of antiferromagnetic exchange interaction between  $\text{Fe}^{3+}$  ions.

DOI: 10.1103/PhysRevB.74.174419

PACS number(s): 75.10.Pq, 75.30.Cr, 75.60.Ej, 75.30.Hx

## I. INTRODUCTION

Low dimension materials are currently in limelight due to their anisotropic electronic and magnetic properties.<sup>1</sup> For example, Haldane<sup>2</sup> has predicted that the one-dimensional (1D) Heisenberg antiferromagnets, described by the Hamiltonian:  $H = \sum_i J \mathbf{S}_i \cdot \mathbf{S}_{i+1}$ , have different behavior for integer and noninteger values of the spins. In the former case, the ground state is separated from the excited state by an energy gap while the latter does not show any energy gap. Among the low dimensional materials, quasi-one-dimension compounds of type  $A_3MXO_6$  [ $A = \text{Ca}, \text{Sr}$  and  $(M, X) = \text{alkali or transition metal ions}$ ] have recently attracted a lot of interest.<sup>3-24</sup> These compounds crystallize in the  $\text{K}_4\text{CdCl}_6$  (rhombohedral) type structure with space group  $R\bar{3}c$ . Crystal structure of these compounds consists of chains of alternating face-sharing  $\text{MO}_6$  trigonal prism (TP) and  $\text{XO}_6$  octahedra (OCT) along the crystallographic  $c$  axis (Fig. 1). These chains are linear if no structural distortion exists at  $\text{MO}_6$  trigonal prism and  $\text{XO}_6$  octahedra. The  $\text{K}_4\text{CdCl}_6$  type rhombohedral structure undergoes a monoclinic distortion if ions at  $(M, X)$  position are Jahn-Teller ions. For example  $\text{Sr}_3\text{CuPtO}_6$  crystallizes in the monoclinic structure (space group  $C2/c$ ) due to the presence of  $\text{Cu}^{2+}$  (Jahn-Teller) cation at the  $M$  site<sup>4</sup> resulting in the zigzag arrangement of Cu and Pt ions along the  $c$  axis. For the rhombohedral structure, these linear spin chains of  $(M, X)$  ions are arranged on a triangular lattice in the  $ab$  plane and each chain is surrounded by six chains. These linear spin chains are separated by nonmagnetic  $A^{2+}$  ions. One-dimensional character in magnetic properties for these compounds is expected because distance between the magnetic ions along the chain is approximately half that of the interchain distance ( $5.24 \text{ \AA}$  for  $\text{Ca}_3\text{Co}_2\text{O}_6$ ). Geometrical frustration in these compounds with a triangular lattice of spin chains is expected if the spins are Ising type (aligned along the crystallographic  $c$  axis) and interchain interaction is antiferromagnetic (AFM). Many compounds of the afore-said series have been synthesized and their magnetic properties have been studied from the point of view of one-

dimension magnetism. Among these compounds,  $\text{Ca}_3\text{Co}_2\text{O}_6$  has attracted a lot of attention due to its peculiar magnetic properties.<sup>5-20</sup> In this compound both the  $\text{Co}^{3+}$  ions located at OCT and TP sites in this compound, are in the trivalent electronic state, but due to the different crystalline electric fields, they are in the different spin states [high spin (HS) state ( $S=2$ ) at the TP site and low spin (LS) state ( $S=0$ ) at the OCT site].<sup>5,6</sup> Some of the important features<sup>5-22</sup> of this compound are (i) strong Ising nature of the spins along the chain, (ii) ferromagnetic (FM) intrachain interaction, (iii) AFM interchain interaction (which combines with the triangular lattice arrangement of the chains and gives rise to a geometrical frustration), (iv) at 25 K it undergoes to a partially disordered antiferromagnetic (PDA) state, where two third of the chains are coupled antiferromagnetically while the one third is left disordered, (v) at 7 K it shows a spin freezing state, and (vi) below 7 K, a sequence of regularly spaced steps in the dc magnetization ( $M$ ) versus magnetic field ( $H$ ) curve is observed which is taken as the signature of the quantum tunneling of magnetization (QTM).<sup>19</sup>

Since the electrical and magnetic properties of oxides with this type of structure strongly depend on the spin and

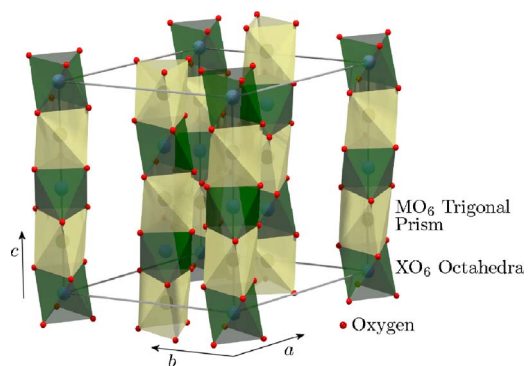


FIG. 1. (Color online) Schematic diagram of  $A_3MXO_6$  type compounds. For clarity oxygen atoms are shown smaller in size and other atoms are not marked.

valence states of transition metal, a large number of opportunities exist to modify these physical properties by tuning intrachain and interchain interactions in this compound by a suitable substitution at the Co site of  $\text{Ca}_3\text{Co}_2\text{O}_6$ . For example, Kageyama *et al.*<sup>23</sup> carried out the Mössbauer study on Fe doped  $\text{Ca}_3\text{Co}_2\text{O}_6$  compound ( $\text{Ca}_3\text{Co}_{2-x}\text{Fe}_x\text{O}_6$  with  $x=0.02$  alone). Arai *et al.*<sup>24</sup> reported the results of their temperature dependent (over  $\sim 2-30$  K) zero field-cooled and field-cooled dc magnetization under 1 kOe external magnetic field and Mössbauer measurements on  $\text{Ca}_3\text{Co}_{2-x}\text{Fe}_x\text{O}_6$  compounds to study the effect of  $\text{Fe}^{57}$  impurity up to a maximum  $x$  value of 0.1. However, systematic study on these iron-doped compounds has not been reported in the literature so far. Here we report the effect of iron doping at the Co site on the structural and magnetic properties of  $\text{Ca}_3\text{Co}_2\text{O}_6$ . The choice of iron to tune intrachain and interchain magnetic interactions was motivated because the ionic radii of  $\text{Co}^{3+}$  and  $\text{Fe}^{3+}$  with six oxygen coordination are very close (0.61 and 0.645 Å, respectively<sup>25</sup>). No strong lattice effect will, therefore, be introduced, and changes only due to the different electronic structures of  $\text{Co}^{3+}$  and  $\text{Fe}^{3+}$  are expected. Moreover, the present study deals with the mixed Ising (Co) and Heisenberg (Fe) spin chains system. We believe that the result of the present experimental study would be of great importance to develop the theory for these types of quasi-1D spin chain systems.

## II. EXPERIMENTAL

Polycrystalline samples of  $\text{Ca}_3\text{Co}_{2-x}\text{Fe}_x\text{O}_6$  ( $x=0, 0.1, 0.2$ , and  $0.4$ ) were prepared by solid state reaction method. The required amounts of reagents, CaO,  $\text{Co}_3\text{O}_4$ , and  $\text{Fe}_2\text{O}_3$  were intimately mixed using an agate mortar pestle and placed in alumina crucibles. These powders were calcined at  $800^\circ\text{C}$  for 24 h and then pressed in the form of bars under  $2\text{ ton/cm}^2$  and subsequently heated at  $1000^\circ\text{C}$  for 48 h with intermediate grindings.

Powder x-ray diffraction (XRD) measurements were performed on all the samples at room temperature using Cu  $K\alpha$  radiation from scattering angle ( $2\theta$ )  $10^\circ$  to  $90^\circ$  in equal  $2\theta$  steps of  $0.02^\circ$  [covering a scattering vector  $Q$  ( $=4\pi \sin \theta/\lambda$ ) range of  $0.71$  to  $5.77\text{ \AA}^{-1}$ ].

Neutron diffraction patterns were recorded at room temperature with the five linear position sensitive detector (PSD) based powder diffractometer ( $\lambda=1.249\text{ \AA}$ ) at Dhruva research reactor, Trombay from scattering angle  $6^\circ$  to  $138^\circ$  covering a  $Q$  range of  $0.53$  to  $9.398\text{ \AA}^{-1}$ . Neutron diffraction patterns were converted in equal  $2\theta$  steps of  $0.02^\circ$  using the standard procedure.

The dc magnetization measurements were carried out on all the samples using a commercial (Oxford Instruments) vibrating sample magnetometer. For the zero-field-cooled (ZFC) magnetization measurements, the samples were first cooled from room temperature down to 2 K in zero field. After applying the magnetic field of 1 kOe at 2 K, the magnetization was measured in the warming cycle with the field on. Whereas, for the field-cooled (FC) magnetization measurements, the samples were cooled down to 2 K in the same field (1 kOe) and the FC magnetization was measured in the

warming cycle under the same field. The hysteresis curves were recorded at 1.5 K over  $+110$  to  $-110$  kOe applied field.

Mössbauer spectra for all samples were measured at room temperature using a conventional constant acceleration spectrometer in transmission geometry. A  $\gamma$ -ray source of  $^{57}\text{Co}$  in Rh matrix at room temperature was used. An  $\alpha$ -Fe absorber was used at room temperature to calibrate the Doppler velocity  $V$  and also as the standard for the isomer shift (IS).

## III. RESULTS AND DISCUSSION

### A. Structural characterization

The x-ray and the neutron powder diffraction patterns, recorded at 297 K, are shown in the Figs. 2 and 3, respectively. The diffraction patterns were analyzed by the Rietveld refinement technique using the FULLPROF program.<sup>26</sup> Both the x-ray and the neutron diffraction patterns for each composition were refined simultaneously. In the Rietveld refinement of the neutron diffraction pattern, coherent scattering lengths ( $b_{\text{coh}}$ )  $0.470 \times 10^{-12}$ ,  $0.249 \times 10^{-12}$ ,  $0.945 \times 10^{-12}$ , and  $0.580 \times 10^{-12}$  cm for Ca, Co, Fe, and O, respectively, have been used. The refinement confirms that these compounds crystallize in the rhombohedral structure (space group  $R\bar{3}c$ ). There are six formula units per unit cell. The refinement also confirms that for all iron doped compounds entire Fe is located at the TP site,  $6a$  (0, 0,  $1/4$ ), with no trace of unreacted Fe. In these compounds, Fe/Co ions, therefore, form the linear chain along the crystallographic  $c$  axis. The refined unit cell parameters and other structural parameters are given in Table I. Figure 4 depicts the Fe doping dependence of the lattice constants and the unit cell volume. Selected interatomic distances and bond angles (along the chain and between the chains) are shown in Fig. 5 and their values are given in Table II. The values of the cell constants, interatomic distances and bond angles obtained for the undoped compound  $\text{Ca}_3\text{Co}_2\text{O}_6$  match well with values reported in the literature.<sup>8</sup> It is evident that there is no significant change in the lattice parameters (only slight increase in lattice constant  $a$ ), unit cell volume, bond angles, and bond lengths by Fe doping.

### B. Mössbauer study

Mössbauer spectra for  $\text{Ca}_3\text{Co}_{2-x}\text{Fe}_x\text{O}_6$  ( $x=0.1, 0.2$ , and  $0.4$ ) at room temperature are shown in Fig. 6. All spectra have been fitted well with an asymmetric doublet. Analysis of these spectra gives the quadruple splitting  $|QS|$ : 1.21, 1.23, 1.23 mm/s and isomer shift (IS): 0.41, 0.40, and 0.40 mm/s for  $x=0.1, 0.2$ , and  $0.4$  samples, respectively. In the literature, the similar values of IS for HS  $\text{Fe}^{3+}$  have been reported; 0.35, 0.39, and 0.43 mm/s for  $\text{LiFe}_{0.5}\text{Mn}_{1.5}\text{O}_4$ ,<sup>27</sup>  $\alpha$ - $\text{LiF}_5\text{O}_8$ ,<sup>28</sup> and  $\text{Ca}_3\text{FeRhO}_6$ ,<sup>29</sup> respectively. The QS values, observed for our compounds, are similar to the values reported in the literature for HS  $\text{Fe}^{3+}$  at TP site in the same class of compounds; 1.13 mm/s for  $\text{Ca}_3\text{FeRhO}_6$  (Ref. 29) and 1.23 mm/s for  $\text{Ca}_3(\text{Co}_{0.99}\text{Fe}_{0.01})_2\text{O}_6$ .<sup>23</sup> For HS  $\text{Fe}^{3+}$  in the  $\text{FeO}_6$  OCT, the reported QS values, are 0.02, 0.58, and

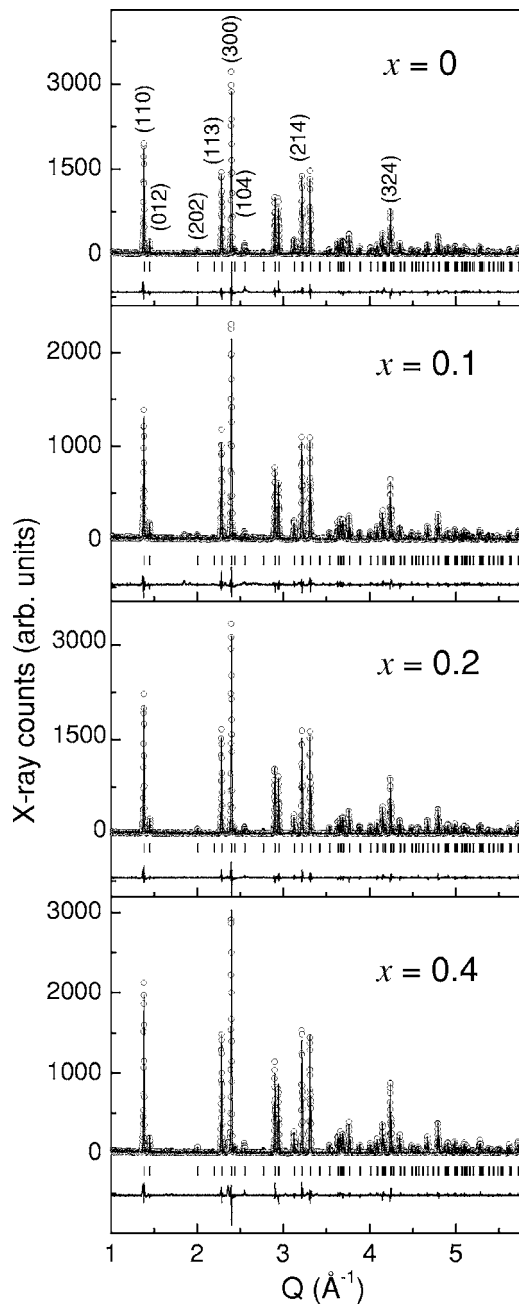


FIG. 2. Observed (open circles) and calculated (solid lines) x-ray diffraction patterns of  $\text{Ca}_3\text{Co}_{2-x}\text{Fe}_x\text{O}_6$  ( $x=0,0.1,0.2,0.4$ ) at 297 K. Solid line at the bottom of each panel show difference between observed and calculated patterns. Vertical lines show the position of Bragg peak. The  $(hkl)$  values corresponding to stronger Bragg peaks are also listed.

0.75 mm/s for  $\alpha\text{-LiF}_5\text{O}_8$ ,<sup>28</sup>  $\alpha\text{-LiFeO}_2$ ,<sup>30</sup>  $\text{LiFe}_{0.5}\text{Mn}_{1.5}\text{O}_4$ ,<sup>27</sup> respectively which are much lower than our experimentally observed values. Therefore, possibility of  $\text{Fe}^{3+}$  going at octahedral site can be ruled out. From the observed value of IS and QS we can conclude that HS  $\text{Fe}^{3+}$  is doped at the TP (Co2) site. This result (Fe is doped at the TP site) is consistent with the outcome of our Rietveld refinement of x-ray and neutron diffraction data.

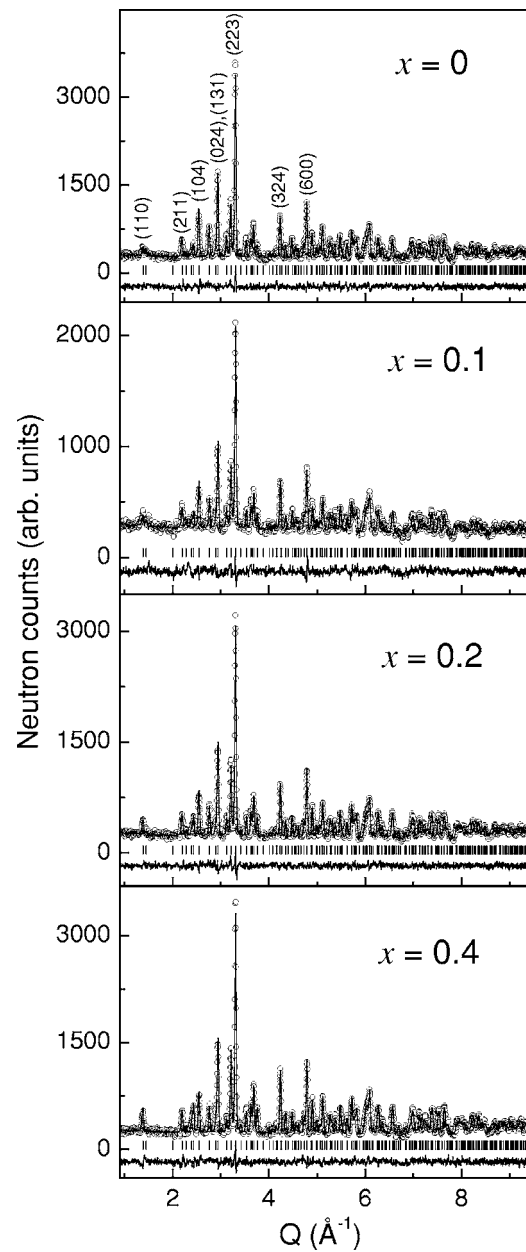


FIG. 3. Observed (open circles) and calculated (solid lines) neutron diffraction patterns of  $\text{Ca}_3\text{Co}_{2-x}\text{Fe}_x\text{O}_6$  ( $x=0,0.1,0.2,0.4$ ) at 297 K. Solid line at the bottom of each panel show difference between observed and calculated patterns. Vertical lines show the position of Bragg peak. The  $(hkl)$  values corresponding to stronger Bragg peaks are also listed.

### C. dc-magnetization study

#### 1. ZFC and FC magnetization vs temperature

The temperature dependence of the ZFC and FC dc magnetization for all samples under  $H=1$  kOe is shown in Fig 7. Inverse magnetic susceptibility vs temperature has been plotted in the inset of Fig 7. It is clear from Fig. 7 that the high temperature magnetic susceptibility obeys the Curie-Weiss law [ $\chi_{\text{mol}}=C_{\text{mol}}/(T-\theta_p)$ ]. Here  $C_{\text{mol}}$  is molar Curie constant and  $\theta_p$  is the paramagnetic Curie temperature. The value of  $\theta_p$  decreases as the concentration of iron increases; reaching

TABLE I. Atomic positions, lattice constants, and thermal parameters for  $\text{Ca}_3\text{Co}_{2-x}\text{Fe}_x\text{O}_6$  samples. All crystallographic sites are fully occupied.

$x$	Atom	Site	$x$	$y$	$z$	$B_{\text{iso}}$
0	Ca	18e	0.3698(2)	0	$\frac{1}{4}$	0.39 (4)
	Co1	6b	0	0	0	0.37 (8)
	Co2	6a	0	0	$\frac{1}{4}$	0.48 (9)
	O	36f	0.1774(4)	0.0257 (5)	0.1145 (3)	0.53 (2)
0.1	Ca	18e	0.3697(6)	0	$\frac{1}{4}$	0.40 (5)
	Co1	6b	0	0	0	0.38 (9)
	Co2	6a	0	0	$\frac{1}{4}$	0.34 (9)
	Fe	6a	0	0	$\frac{1}{4}$	0.49 (8)
0.2	O	36f	0.1779(6)	0.02377(6)	0.1133(6)	0.73 (4)
	Ca	18e	0.3693(3)	0	$\frac{1}{4}$	0.49 (4)
	Co1	6b	0	0	0	0.45 (8)
	Co2	6a	0	0	$\frac{1}{4}$	0.5 (2)
0.4	Fe	6a	0	0	$\frac{1}{4}$	0.5 (4)
	O	36f	0.1765(2)	0.0238(2)	0.1138(2)	0.69 (3)
	Ca	18e	0.3692(2)	0	$\frac{1}{4}$	0.55 (4)
	Co1	6b	0	0	0	0.39 (9)
	Co2	6a	0	0	$\frac{1}{4}$	0.54 (7)
	Fe	6a	0	0	$\frac{1}{4}$	0.49 (7)
	O	36f	0.1759(3)	0.0235(3)	0.1139(2)	0.85 (4)

17.6 and 7.5 K for  $x=0.1$  and  $0.2$ , respectively against  $\theta_p = 27.9$  K for  $x=0$  and it becomes negative ( $-1.6$  K) for  $x=0.4$  sample, which indicates that at this higher concentration of iron, AFM interaction dominates over FM interaction.

The effective paramagnetic moment  $\mu_{\text{eff}}$   $[=(3C_{\text{mol}}k_B/N_A\mu_B^2)^{1/2} \approx (8C_{\text{mol}})^{1/2}]$ , where  $k_B$  stands for Boltzmann constant and  $N_A$  stands for Avogadro number, obtained from the slope of  $\chi^{-1}$  vs  $T$  curves, are depicted in Fig. 8. Theoretically expected (spin only) values of the  $\mu_{\text{eff}}$  using the expression  $\mu_{\text{eff}} = [(1-x)g\sqrt{S_{\text{Co(TP)}}(S_{\text{Co(TP)}}+1)} + xg\sqrt{S_{\text{Fe(TP)}}(S_{\text{Fe(TP)}}+1)}]\mu_B$  with  $g=2$  are also shown in Fig. 8. Here  $\mu_{\text{eff}}$  has been calculated (assuming spin only contribution) by considering  $\text{Co}^{3+}$  at OCT site in the LS state ( $S=0$ ),  $\text{Co}^{3+}$  at TP site in the HS state ( $S=2$ ), and  $\text{Fe}^{3+}$  at TP site in the HS state ( $S=5/2$ ).<sup>23</sup> For the parent compound

$\text{Ca}_3\text{Co}_2\text{O}_6$ , experimental value ( $4.8 \mu_B$  per formula unit) matches with the theoretical value ( $4.89 \mu_B$  per formula unit) and for iron doped samples, experimental  $\mu_{\text{eff}}$  values are higher than theoretically expected values. If we assume that orbital moment of  $\text{Co}^{3+}$  is not quenched in the TP site (orbital moment of  $\text{Fe}^{3+}$  is zero since it has half filled  $3d$  shell), the calculated values of  $\mu_{\text{eff}}$  are higher than the observed values (Fig. 8). If we consider that orbital momentum is partially quenched, theoretical value of the  $\mu_{\text{eff}}$  (considering different values of  $L$ ) do not match with the experiment values. Another possibility of observing higher experimental

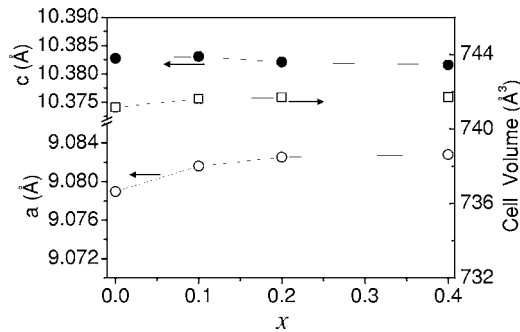


FIG. 4. Lattice constants and unit cell volume for  $\text{Ca}_3\text{Co}_{2-x}\text{Fe}_x\text{O}_6$  as a function of iron content. Solid lines are guides to the eye.

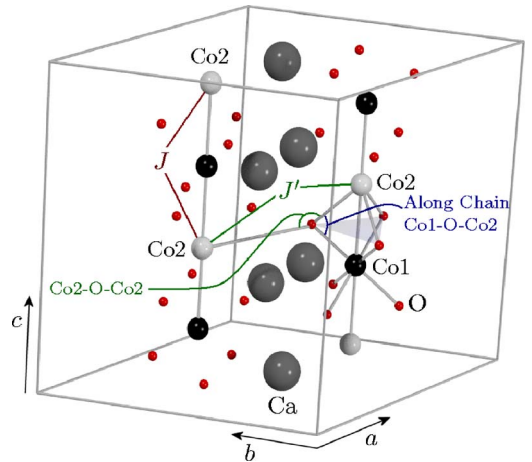


FIG. 5. (Color online) Unit cell of  $\text{Ca}_3\text{Co}_{2-x}\text{Fe}_x\text{O}_6$ , showing selected (Co1-O-Co2 and Co2-O-Co2) bond angles. Paths of inter-chain and intra-chain exchange interactions are also shown as  $J'$  and  $J$ , respectively. Only selected atoms are shown for clarity.

TABLE II. Selected bond lengths and bond angles for  $\text{Ca}_3\text{Co}_{2-x}\text{Fe}_x\text{O}_6$  samples.

x	Bond	Length (Å)		Bond angle	
		along the chain			
0	Ca-O	2.345(5)	2.459(2)	Co1-O-Co2	81.14(9)°
		2.550(3)	2.470(1)		
	Co1-O	1.916(2)	between the chains		
	Co2-O	2.070(1)			
	Co1-Co2	2.59569			
	Co2-O	3.905(2)			
0.1	Ca-O	2.339(4)	2.452(3)	Co1-O-Co2	80.8(1)°
		2.476(3)	2.548(3)		
	Co1-O	1.919(3)	between the chains		
	Co2-O	2.079(3)			
	Co1-Co2/Fe	2.59570			
	Co2-O	3.903(3)			
0.2	Ca-O	2.393(2)	2.463(2)	Co1-O-Co2	81.25(3)°
		2.474(1)	2.552(3)		
	Co1-O	1.920(2)	between the chains		
	Co2-O	2.067(2)			
	Co1-Co2/Fe	2.59572			
	Co2-O	3.912(1)			
0.4	Ca-O	2.346(3)	2.468(2)	Co1-O-Co2	81.48(9)°
		2.551(3)	2.468(2)		
	Co1-O	1.922(2)	between the chains		
	Co2-O	2.062(2)			
	Co1-Co2	2.59573			
	Co2-O	3.918(2)			
Co1-Co2	5.52203				

values of effective paramagnetic moment as compared to the theoretically expected spin only values for Fe doped compounds may be LS to HS transition of octahedral  $\text{Co}^{3+}$  ions that are located near  $\text{Fe}^{3+}$  ions,<sup>31</sup> which could also be responsible for the slight increase of cell constants for the present Fe doped compounds. Increase of cell parameters by such a spin transition has been reported in the literature.<sup>31</sup> Such a transition is possible<sup>31</sup> because covalency of the Fe-O bond is higher than the covalency of Co-O bond (i.e., electronegativity of  $\text{Fe}^{3+}$  is higher than that of  $\text{Co}^{3+}$ ; 1.9, and 1.8, respectively<sup>32</sup>). Under the framework of spin transition for  $\text{Co}^{3+}$  at the octahedral site, the  $\mu_{\text{eff}}$  can be calculated using the expression

$$\mu_{\text{eff}} = [(1-x)g\sqrt{S_{\text{Co(TP)}}(S_{\text{Co(TP)}}+1)} + xg\sqrt{S_{\text{Fe(TP)}}(S_{\text{Fe(TP)}}+1)} + xfg\sqrt{S_{\text{Co(OCT)}}(S_{\text{Co(OCT)}}+1)}]\mu_{\text{B}}$$

with  $g=2$  (Fig. 8). Here  $f$  is the fraction of  $\text{Co}^{3+}$  ions (at the

octahedral site) that undergoes LS to HS transition for each doped  $\text{Fe}^{3+}$  ion. The experimental and the theoretical values match for  $x=0.1$  and  $0.2$  by taking  $f=0.75$  (Fig. 8). For  $x=0.4$  the experimental and the theoretical values match by taking  $f=0.34$ . The observed lower value of  $f$  for the  $x=0.4$  sample can be explained by the fact that for higher concentration of iron, there could be pairs/sequence of  $\text{Fe}^{3+}$  ions along the chain, so the effective number of  $\text{Co}^{3+}$  ions (with  $\text{Fe}^{3+}$  ions as nearest neighbors) showing transition from LS to HS is small. For the parent compound  $\text{Ca}_3\text{Co}_2\text{O}_6$ , there is a sudden increase in the magnetization at around 25 K and also there exist a peak in the magnetization at around 10 K. These observations are consistent with the reported results for this compound.<sup>4-6</sup> In the literature, two kinds of magnetic exchange interactions have been considered in this chain compound.<sup>17</sup> The exchange interaction  $J$  between the magnetic Co2 ions located at TP site along the chain axis ( $c$  axis) is FM and the superexchange interaction  $J'$  between the

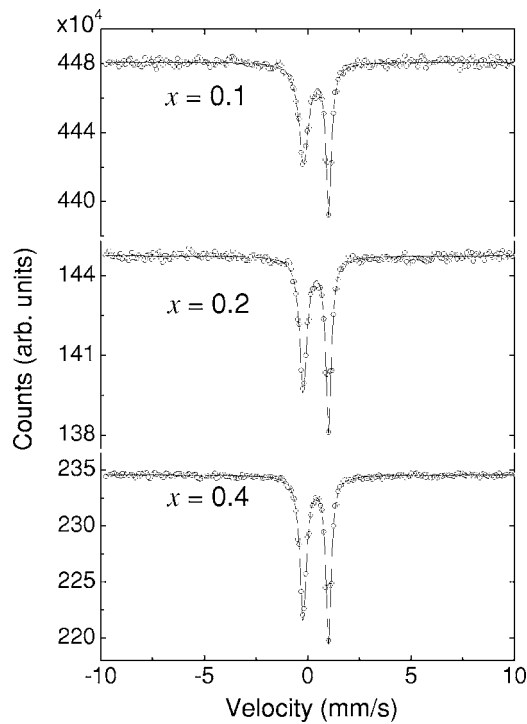


FIG. 6. Mössbauer spectra for  $\text{Ca}_3\text{Co}_{2-x}\text{Fe}_x\text{O}_6$  ( $x=0.1, 0.2, 0.4$ ) at room temperature. Solid lines are the fitted curves.

magnetic  $\text{Co}^{2+}$  ions (via oxygen ions) is AFM (Fig. 5). Sudden increase in the magnetization at around 25 K has been ascribed in the literature<sup>4–20</sup> as due to the combined effect of FM ordering along the chain and AFM ordering between the chains. This argument is supported by the simultaneous appearance of AFM and FM Bragg peaks in the neutron diffraction pattern at  $T \sim 25$  K (Refs. 21 and 22) and sharp peak in the specific heat (under zero fields)<sup>9</sup> at the same temperature. This type of spin configuration has been described as the onset of the PDA state and it is supported by the muon spin relaxation study.<sup>33</sup> While peak in the magnetization curve at around 10 K is considered as an indicative of magnetic transition to the ferrimagnetic (FIM) state.<sup>34</sup>

From the temperature dependence of FC and ZFC dc magnetization (shown in Fig. 7) it is evident that for all the samples a bifurcation between FC and ZFC magnetization is found at lower temperatures. This bifurcation in FC and ZFC magnetization may be taken as the signature of geometrical frustration due to triangular lattice of Ising Co moments in the  $ab$  plane. Results of the reported low temperature Mössbauer study<sup>24</sup> show that  $\text{Fe}^{3+}$  remains in the paramagnetic state in the FM ordered chains below 25 K. Figure 7 also indicates that as the concentration of iron increases, magnetization decreases. This decrease in the magnetization and  $\theta_p$  (negative for  $x=0.4$ ) indicates that as the doping of iron increases the long range FM ordering along the chain is reduced (due to reduced correlation length between Co moments along the chain) and AFM interchain interaction dominates over the FM intrachain interaction. The reason behind this has been ascribed due to different magnetic character of Co host (Ising) and Fe impurity (Heisenberg) spins.<sup>23</sup>

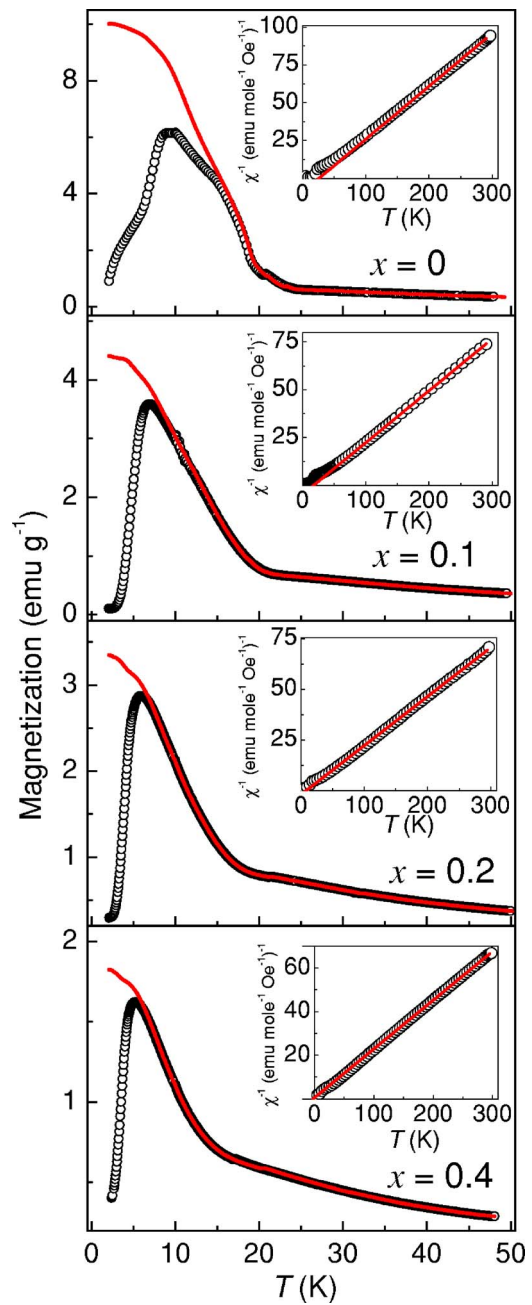


FIG. 7. (Color online) dc magnetization vs temperature curves under 1 kOe field for  $\text{Ca}_3\text{Co}_{2-x}\text{Fe}_x\text{O}_6$  ( $x=0, 0.1, 0.2, 0.4$ ). The open circles and the solid line correspond to ZFC and FC modes, respectively. Insets show inverse dc susceptibility vs temperature curves fitted with the Curie-Weiss law.

Figure 9 depicts the temperature dependence of molar susceptibility, where  $\chi T$  vs  $T$  is plotted. It reveals four main features (i) in the high temperature range (150–300 K)  $\chi T$  approaches its paramagnetic limit, (ii) as temperature is decreased below the 150 K,  $\chi T$  starts increasing giving the signature of short range ordering along the chains, (iii) further decreasing the temperature, a dip in  $\chi T$  vs  $T$  plot is found. The temperature corresponding to the dip varies with  $x$  (24.83 K for  $x=0$  and 3.59 K for  $x=0.4$ ). This dip in  $\chi T$  vs  $T$  plot may be ascribed as FIM ordering at low

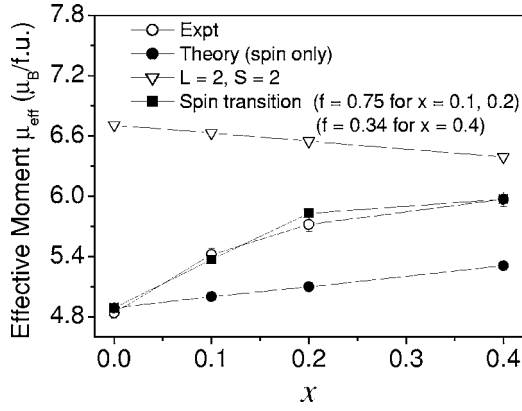


FIG. 8. Theoretical and experimental  $\mu_{\text{eff}}$  vs iron concentration. Solid lines are guide to the eye.

temperatures,<sup>35</sup> and (iv) sharp increase in  $\chi T$  below the dip temperature and then again decreases at lower temperatures down to 2 K. The decrease in the  $\chi T$  at low temperature ( $T < 7$  K) has been assigned to a three dimension ordering (3D) in the literature<sup>36</sup> for the undoped compound.

## 2. Intrachain and interchain exchange interactions

The intrachain exchange constant can be determined by fitting the experimental  $\chi T$  vs  $T$  curves.<sup>36,37</sup> Theoretical studies show that the parallel<sup>36</sup> and the perpendicular<sup>38</sup> susceptibilities for  $S=2$  1D Ising spin chain are given by

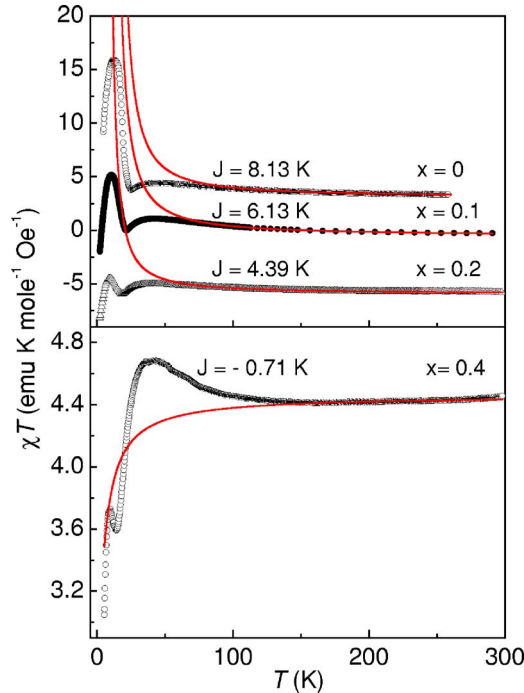


FIG. 9. (Color online) Plots of  $\chi T$  vs  $T$  for  $\text{Ca}_3\text{Co}_{2-x}\text{Fe}_x\text{O}_6$  ( $x = 0, 0.1, 0.2, 0.4$ ) derived from FC magnetization curves. Solid lines represent the fitted curve using Eq. (3). For  $x=0.1$  and  $0.2$ ,  $\chi T$  values are shifted down by 5 and 10 ( $\text{emu K mol}^{-1} \text{Oe}^{-1}$ ), respectively for clarity.

TABLE III. Magnetic exchange constants for  $\text{Ca}_3\text{Co}_{2-x}\text{Fe}_x\text{O}_6$  samples.

$x$	$J(\text{K})$	$J'(\text{K})$	$ J'/J $
0	8.13	-0.20	0.025
0.1	6.13	-0.27	0.044
0.2	4.39	-0.30	0.068
0.4	-0.71	-0.32	0.451

$$\chi_{\parallel} T = \frac{3}{4} g^2 \exp(8J/k_B T) \quad (1)$$

and

$$\chi_{\perp} T = \frac{3}{4} g^2. \quad (2)$$

Here  $g$  is the Lande factor and  $k_B$  stands for the Boltzmann constant.  $J$  is the intrachain exchange constant. For polycrystalline (powder) sample, susceptibility can therefore be written as

$$\chi_p T = 1/3 \chi_{\parallel} T + 2/3 \chi_{\perp} T. \quad (3)$$

Equation (3) is strictly valid for the  $S=2$  Ising spin chain. But our system (except  $\text{Ca}_3\text{Co}_2\text{O}_6$ ) is not  $S=2$ , 1D Ising spin chain system (for  $\text{Fe}^{3+}$  ions, value of  $S$  is  $5/2$ ). In the literature no theoretical expression is available for  $S=2$  and  $S=5/2$  mixed spin system. We have therefore, used Eq. (3) to estimate approximate value of exchange constant  $J$ . This type of approximate method has already been used in the literature<sup>18</sup> for  $\text{Ca}_3\text{Co}_{2-x}\text{Cr}_x\text{O}_6$ , where  $\text{Co}^{3+}$  is in the HS and the LS state in the TP and OCT, respectively and  $\text{Cr}^{3+}$  at the OCT site is in the HS ( $S=3/2$ ) state. By fitting the higher temperature part of  $\chi_p T$  vs  $T$  curve using Eq. (3) (Fig. 9) as per the procedure followed in the literature,<sup>18</sup> we have estimated the value of intrachain exchange constant  $J$  (shown in Table III). It is found that as the concentration of iron increases,  $J$  decreases. For instance as  $x$  increases from 0 to 0.2,  $J$  decreases from 8.1 to 4.3 K and for  $x=0.4$  it becomes negative ( $J=-0.7$  K). Positive value of  $J$  refers that intrachain interaction is FM while negative value of  $J$  indicates that interaction is AFM. The derived negative value of  $J$  for the  $x=0.4$  sample is consistent with the negative value of  $\theta_p$  for this sample. Here we give some physical argument to explain the negative value of  $J$ . For  $\text{Ca}_3\text{Co}_{2-x}\text{Fe}_x\text{O}_6$ , when concentration of Fe is low (small value of  $x$ ), the probability of having Fe pairs or clusters in a Co chain is very small and  $\text{Fe}^{3+}$  ions are mainly isolated. For small value of  $x$ , iron limits the correlation length by breaking FM order between  $\text{Co}^{3+}$  ions along the  $c$  axis and reduces the strength of intrachain exchange coupling constant  $J$ . When  $x$  increases ( $>0.2$ ), formation of pairs of  $\text{Fe}^{3+}$  ions along the chain is probable. There may be AFM exchange interaction (via oxygen) between  $\text{Fe}^{3+}$  ions along the chain (Fig. 5) which can give the negative value of  $J$ . This can lead to a FIM ordering (with negative  $\theta_p$ ) at lower temperatures. Low temperature neutron diffraction is necessary to confirm these findings. However, at our research center at present we are limited to

a lowest temperature of about 20 K for neutron diffraction study, which restricts us to perform the required low temperature neutron diffraction experiments.

Interactions between the chains in the  $ab$  plane give deviation from the 1D spin system. The deviation from the ideal 1D character of Ising chain can be taken into account by introducing the mean field correction to the ideal 1D Ising spin model. Mean field correction to the  $S=1/2$ , 1D Ising spin chain is available in the literature and it has been used<sup>39</sup> to evaluate the interchain exchange constant. However, in the literature no mean field expressions, either for  $S=2$  Ising spin chain or for  $S=2$  and  $S=5/2$  mixed spin system, exist. It will be of great importance to evaluate the interchain interaction if the mean field corrections for such spin systems are available. An alternate option to calculate interchain interaction is by using ferri- to ferro-magnetic transition field ( $H_{\text{FIM-FM}}$ ). A field induced FIM to FM-like transition is found in our  $M$  vs  $H$  study (Fig. 10). In a model of Ising spin chain, interchain interaction is related to  $H_{\text{FIM-FM}}$  through the relation  $J' = \frac{g\mu_B H_{\text{FIM-FM}}}{12S}$ .<sup>18</sup> For the present system of mixed spins ( $S=2$  and  $S=5/2$ ), assuming  $S=2$  and  $g=2$ , we have derived the value of  $J'$  as used for  $S=2$  and  $S=3/2$  mixed spin chain system in the literature.<sup>18</sup> The value of  $J'$  varies from  $-0.20$  K for  $x=0$  to  $-0.32$  K for  $x=0.4$ . Therefore, as the concentration of iron increases from 0 to 0.4, interchain interaction increases. Since the distance between the magnetic ions perpendicular to the chain axis and the bond angle via oxygen do not change by iron doping, the increase in the value of  $J'$  can be understood by assuming that strength of exchange coupling for Co2/Fe-O-Co2/Fe pathway is greater than that of the Co2-O-Co2. This is consistent with the fact that Fe is known to introduce negative exchange interactions. Fe<sup>3+</sup> has five electrons in the  $d$  orbital, while Co<sup>3+</sup> has six and also spin character of host (Co) is Ising while impurity (Fe) is of Heisenberg nature. The ratio  $\frac{J'}{J}$  characterizes the “one dimensionality” of the magnetic system. It varies from 0.025 for  $x=0$  to 0.451 for  $x=0.4$  as shown in the Table III. In the literature, Clardige *et al.* reported  $\frac{J'}{J} \sim 0.33$  for Sr<sub>3</sub>CuPtO<sub>6</sub> (Heisenberg chain compound)<sup>40</sup> and they concluded that it should not be considered as 1D magnetic system due to a higher value of  $\frac{J'}{J}$ . Since for the present  $x=0.4$  compound  $\frac{J'}{J} \sim 0.451$ , this compound should also not be considered as 1D magnetic system. The  $\frac{J'}{J}$  ratio is very small for Ca<sub>3</sub>Co<sub>2</sub>O<sub>6</sub> hence it has predominantly a one dimension character. We can therefore conclude that as the concentration of iron increases, the one dimensional character of Ising spin chains is reduced.

Previous reports by Flahaut *et al.* on substitution of Co<sup>3+</sup> by Cr<sup>3+</sup> in Ca<sub>3</sub>Co<sub>2</sub>O<sub>6</sub> (Ref. 18) shows that as the concentration of Cr increases from  $x=0$  to  $x=0.1$  in Ca<sub>3</sub>Co<sub>2-x</sub>Cr<sub>x</sub>O<sub>6</sub>, both  $J$  and  $J'$  decrease. Here we would like to point out that effects of substitution of Cr are much different from the present study where Fe is doped. Cr<sup>3+</sup> substitutes the LS Co<sup>3+</sup> at octahedral site and it is in the HS state ( $S=3/2$ ). In Ca<sub>3</sub>Co<sub>2-x</sub>Cr<sub>x</sub>O<sub>6</sub>, solubility range of Cr<sup>3+</sup> is limited to about 10 at. % occupation of octahedral site. In the Cr substitution case, cell constants  $a$  and  $c$  change by  $\sim 0.14\%$  and  $0.08\%$ , respectively for the change in  $x$  from 0 to 0.15, whereas in the present case, the cell constant  $a$  changes only by  $0.01\%$  for change in the  $x$  from 0 to 0.4.

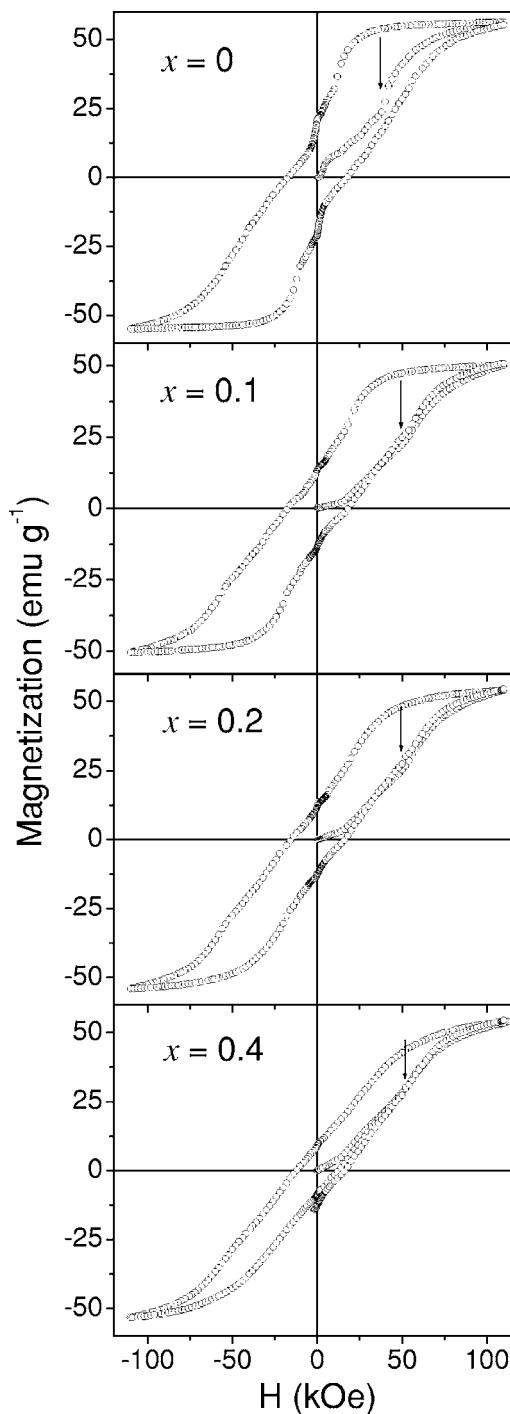


FIG. 10. Hysteresis curves at 1.5 K for Ca<sub>3</sub>Co<sub>2-x</sub>Fe<sub>x</sub>O<sub>6</sub> ( $x=0,0.1,0.2,0.4$ ). Virgin magnetization curves (first leg) show a possible field induced FIM to FM transition (marked by arrows).

### 3. Field dependent magnetization

Figure 10 depicts hysteresis loops (field up to 110 kOe) at 1.5 K for all the samples. It is evident from the figure that virgin magnetization ( $M$ ) varies linearly with field in a small field region. It is also found that large hysteresis exists in  $M$  versus  $H$  curves of all samples but as the concentration of iron increases, these curves become less hysteretic. The magnetization saturates for  $x=0$  but for  $x=0.1, 0.2$ , and  $0.4$

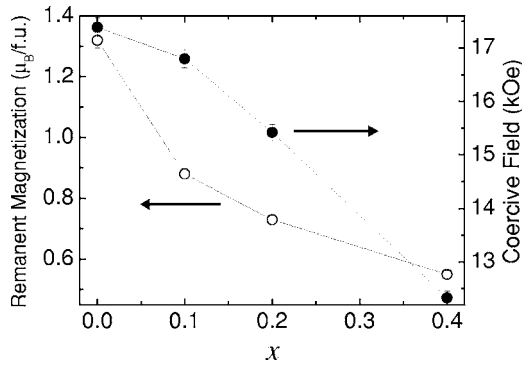


FIG. 11. Variation of remanent magnetization and coercive fields with composition. Solid lines are guide to the eye.

samples the magnetization does not saturate even under the highest applied field. Experimentally observed values of the remanent magnetization and the coercive fields are shown in Fig. 11. It is clear that as the concentration of iron increases both remanent magnetization and coercive field decrease. It is therefore, evident that the magnetic hardness decreases with Fe doping. This is consistent with the observed fact that with increasing Fe doping, the 1D character of Ising spin chains is reduced.

The spatial dimensionality ( $d$ ) of arrangement of magnetic ions in the present system can be deduced from the approach of the magnetization to its saturation value ( $M_S$ ) in the high field region.<sup>41</sup> This dependency is given by

$$\frac{M_S - M}{M_S} \propto (H)^{(d-4)/2}. \quad (4)$$

Here, the proportionality constant is given by  $\delta = (C/M_S)^{(4-d)/2}$  with  $C$  as magnetocrystalline anisotropy constant. According to Eq. (4), approach of magnetization to its saturation value  $\Delta M/M_S$  (here  $\Delta M = M_S - M$ ) obeys  $H^{-3/2}$  and  $H^{-1/2}$  dependence for the 1D and three-dimensional (3D) interaction of magnetic ions, respectively. Figure 12 depicts the variation of  $\Delta M/M_S$  with  $H^{-3/2}$  and  $H^{-1/2}$  for all the samples at 1.5 K. Inset of Fig. 12 depicts variation of anisotropy constant ( $C$ ) with composition, derived from the slope  $[(C/M_S)^{3/2}]$  of  $\Delta M/M_S$  vs  $H^{-3/2}$  curves. The results show that for  $x=0, 0.1, \text{ and } 0.2$  samples,  $\Delta M/M_S$  is proportional  $H^{-3/2}$  and hence imply the 1D character of the spatial arrangement of magnetic ions in these samples. For  $x=0.4$  sample,  $\Delta M/M_S$  deviates from  $H^{-3/2}$  dependence, which can be ascribed as a deviation from ideal 1D character of this sample (consistent with highest derived value of  $J'/J$ ). The decrease of anisotropy constant ( $C$ ) with the increase of iron concentration (inset of Fig. 12) is also consistent with the aforesaid argument.

#### IV. SUMMARY AND CONCLUSIONS

We have prepared single phase polycrystalline samples of quasi-1-D compounds  $\text{Ca}_3\text{Co}_{2-x}\text{Fe}_x\text{O}_6$  ( $x=0, 0.1, 0.2, \text{ and } 0.4$ ). Simultaneous refinement of the neutron and the x-ray diffraction data confirms that Fe is located at the TP site. The values of IS and QS derived from the Mössbauer spectra also

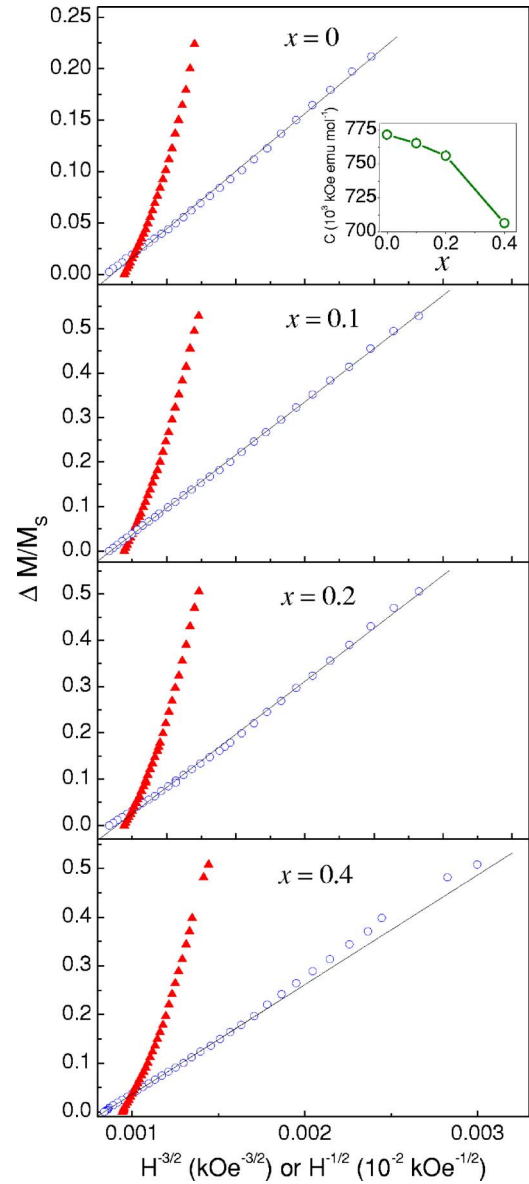


FIG. 12. (Color online) Plots of  $\Delta M/M_S$  vs  $H^{-3/2}$  (open circles) and  $\Delta M/M_S$  vs  $H^{-1/2}$  (solid triangles) obtained from high field region of virgin magnetization curves. Straight lines represent linear fit of  $\Delta M/M_S$  vs  $H^{-3/2}$ . Inset shows variation of anisotropy constant with composition.

confirm that Fe is doped at the TP site and it is in the  $\text{Fe}^{3+}$  HS state. The magnetic properties of  $\text{Ca}_3\text{Co}_2\text{O}_6$  are found to be sensitive to Fe doping. The values of intrachain exchange constant  $J$  derived by fitting the high temperature  $\chi T$  vs  $T$  curves with the theoretical model indicates that as the concentration of iron increases,  $J$  decreases and for higher concentration of iron ( $x > 0.2$ ) it becomes negative. These results can be understood by considering the formation of pairs of  $\text{Fe}^{3+}$  ions along the chain for higher Fe doping concentration and negative exchange interaction between  $\text{Fe}^{3+}$  ions along the chain (via oxygen). Interchain exchange constant  $J'$  derived from the FIM to FM-like transition field indicates that  $J'$  increases with Fe concentration. This indicates that the strength of negative exchange interaction for

Co<sub>2</sub>/Fe-O-Co<sub>2</sub>/Fe pathway is greater than that of the Co<sub>2</sub>-O-Co<sub>2</sub> which can be ascribed to the different spin nature of Co<sup>3+</sup> and Fe<sup>3+</sup> ions. Deviation from  $\Delta M/M_S = \delta H^{-3/2}$  behavior with increasing iron concentration indicates the deviation from quasi-1D character of spins for higher Fe doped compounds. In summary, doping of iron breaks the ferrmagnetically ordered chain and reduces the strength of intrachain positive exchange interaction. It also enhances the strength of interchain negative exchange interaction. Low temperature neutron diffraction and other microscopic measurements are necessary to throw more light on the microscopic nature of magnetic correlation in these compounds. Here it should be noted that these 1D materials are highly anisotropic in terms of electronic spin character. Mag-

netization measurement using powder samples gives average information. Therefore measurements using single crystals are necessary to get the detailed quantitative information.

#### ACKNOWLEDGMENTS

The authors are grateful to S. L. Chaplot, J. V. Yakhmi, and V. C. Sahni for their encouragement and support in this work. A.J. acknowledges the help rendered by P. S. R. Krishna and A. K. Rajarajan in Rietveld refinement and magnetization measurements, respectively. A.J. also acknowledges the help provided by A. B. Shinde and R. Chitra in performing neutron diffraction and x-ray diffraction experiments, respectively.

\*Corresponding author. Email address: smyusuf@barc.gov.in

- <sup>1</sup>K. E. Stitzer, J. Darriet, and H.-C. zur Loye, *Curr. Opin. Solid State Mater. Sci.* **5**, 535 (2001).
- <sup>2</sup>F. D. M. Haldane, *Phys. Lett.* **93A**, 464 (1983); *Phys. Rev. Lett.* **50**, 1153 (1983).
- <sup>3</sup>T. N. Nguyen and H.-C. zur Loye, *J. Solid State Chem.* **117**, 300 (1995).
- <sup>4</sup>S. Majumdar, V. Hardy, M. R. Lees, D. McK. Paul, H. Rous-selière, and D. Grebille, *Phys. Rev. B* **69**, 024405 (2004).
- <sup>5</sup>S. Aasland, H. Fjellvåg, and B. Hauback, *Solid State Commun.* **101**, 187 (1997).
- <sup>6</sup>H. Kageyama, K. Yoshimura, K. Kosuge, M. Azuma, M. Takano, H. Mitamura, and T. Goto, *J. Phys. Soc. Jpn.* **66**, 3996 (1997).
- <sup>7</sup>A. Maignan, C. Michel, A. C. Masset, C. Martin, and B. Raveau, *Eur. Phys. J. B* **15**, 657 (2000).
- <sup>8</sup>H. Fjellvåg, E. Gulbrandsen, S. Aasland, A. Olsen, and B. C. Hauback, *J. Solid State Chem.* **124**, 190 (1996).
- <sup>9</sup>V. Hardy, S. Lambert, M. R. Lees, and D. McK. Paul, *Phys. Rev. B* **68**, 014424 (2003).
- <sup>10</sup>B. Martínez, V. Laukhin, M. Hernando, J. Fontcuberta, M. Parras, and J. M. González-Calbet, *Phys. Rev. B* **64**, 012417 (2001).
- <sup>11</sup>B. Raquet, M. N. Baibich, J. M. Broto, H. Rakoto, S. Lambert, and A. Maignan, *Phys. Rev. B* **65**, 104442 (2002).
- <sup>12</sup>V. Hardy, M. R. Lees, A. Maignan, S. Hébert, D. Flahaut, C. Martin, and D. McK. Paul, *J. Phys.: Condens. Matter* **15**, 5737 (2003).
- <sup>13</sup>R. Vidya, P. Ravindran, H. Fjellvåg, A. Kjekshus, and O. Eriksson, *Phys. Rev. Lett.* **91**, 186404 (2003).
- <sup>14</sup>S. Rayaprol, K. Sengupta, and E. V. Sampathkumaran, *Solid State Commun.* **128**, 79 (2003).
- <sup>15</sup>V. Hardy, M. R. Lees, O. A. Petrenko, D. McK. Paul, D. Flahaut, S. Hébert, and A. Maignan, *Phys. Rev. B* **70**, 064424 (2004).
- <sup>16</sup>E. V. Sampathkumaran, N. Fujiwara, S. Rayaprol, P. K. Madhu, and Y. Uwatoko, *Phys. Rev. B* **70**, 014437 (2004).
- <sup>17</sup>R. Frésard, C. Laschinger, T. Kopp, and V. Eyert, *Phys. Rev. B* **69**, 140405(R) (2004).
- <sup>18</sup>D. Flahaut, A. Maignan, S. Hébert, C. Martin, R. Retoux, and V. Hardy, *Phys. Rev. B* **70**, 094418 (2004).
- <sup>19</sup>V. Hardy, D. Flahaut, M. R. Lees, and O. A. Petrenko, *Phys. Rev. B* **70**, 214439 (2004).

- <sup>20</sup>J. Sugiyama, H. Nozaki, J. H. Brewer, E. J. Ansaldo, T. Takami, H. Ikuta, and U. Mizutani, *Phys. Rev. B* **72**, 064418 (2005).
- <sup>21</sup>O. A. Petrenko, J. Wooldridge, M. R. Lees, P. Manuel, and V. Hardy, *Eur. Phys. J. B* **47**, 79 (2005).
- <sup>22</sup>H. Kageyama, K. Yoshimura, K. Kosuge, X. Xu, and S. Kawano, *J. Phys. Soc. Jpn.* **67**, 357 (1998).
- <sup>23</sup>H. Kageyama, S. Kawasaki, K. Mibu, M. Takano, K. Yoshimura, and K. Kosuge, *Phys. Rev. Lett.* **79**, 3258 (1997).
- <sup>24</sup>J. Arai, H. Shinmen, S. Takeshita, and T. Goko, *J. Magn. Magn. Mater.* **272-276**, 809 (2004).
- <sup>25</sup>R. D. Shannon, *Acta Crystallogr.* **32**, 751 (1976).
- <sup>26</sup>J. Rodríguez-Carvajal and T. Roisnel, FullProf.98 and Win-PLoTR: New Windows 95/NT Applications for Diffraction Commission For Powder Diffraction, International Union for Crystallography, *Newsletter N° 20 (May-August) Summer 1998*.
- <sup>27</sup>H. Shigemura, H. Sakaebe, H. Kageyama, H. Kobayashi, A. R. West, R. Kanno, S. Morimoto, S. Nasu, and M. Tabuchi, *J. Electrochem. Soc.* **148**(7), A730-A736 (2001).
- <sup>28</sup>M. Tabuchi, K. Ado, H. Kobayashi, I. Matsubara, H. Kageyama, M. Wakita, S. Tsutsui, S. Nasu, Y. Takeda, C. Masquelier, A. Hirano, R. Kanno, *J. Solid State Chem.* **141**, 554 (1998).
- <sup>29</sup>S. Niitaka, K. Yoshimura, K. Kosuge, K. Mibu, H. Mitamura, and T. Goto, *J. Magn. Magn. Mater.* **260**, 48 (2003).
- <sup>30</sup>M. Tabuchi, S. Tsutsui, C. Masquelier, R. Kanno, K. Ado, I. Matsubara, S. Nasu, H. Kageyama, *J. Solid State Chem.* **140**, 159 (1998).
- <sup>31</sup>T. Kyōmen, Y. Asaka, and M. Itoh, *Phys. Rev. B* **67**, 144424 (2003) and reference therein.
- <sup>32</sup>L. Pauling, *The Nature of the Chemical Bond* (Cornell University and Ithaca, NY, 1960).
- <sup>33</sup>S. Takeshita, J. Arai, T. Goko, K. Nishiyama, and K. Nagamine, *J. Phys. Soc. Jpn.* **75**, 034712 (2006).
- <sup>34</sup>H. Kageyama, K. Yoshimura, K. Kosuge, H. Mitamura, and T. Goto, *J. Phys. Soc. Jpn.* **66**, 1607 (1997).
- <sup>35</sup>S. I. Ohkoshi and K. Hashimoto, *Phys. Rev. B* **60**, 12820 (1999).
- <sup>36</sup>A. Maignan, V. Hardy, S. Hébert, M. Drillon, M. R. Lees, O. Petrenko, D. McK. Paul, and D. Khomskii, *J. Mater. Chem.* **14**, 1231 (2004).
- <sup>37</sup>H. J. M. de Groot, L. J. de Jongh, R. C. Thiel, and J. Reedijk, *Phys. Rev. B* **30**, 4041 (1984).

- <sup>38</sup>M. F. Thorpe and M. Thomsen, *J. Phys. C* **16**, L237 (1983).
- <sup>39</sup>R. E. Greeney, C. P. Landee, J. H. Zhang, and W. M. Reiff, *Phys. Rev. B* **39**, 12200 (1989).
- <sup>40</sup>J. B. Claridge, R. C. Layland, W. H. Henley, and H.-C. zur Loye, *Chem. Mater.* **11**, 1376 (1999).
- <sup>41</sup>S. Karmakar, S. M. Sharma, M. D. Mukadam, S. M. Yusuf, and A. K. Sood, *J. Appl. Phys.* **97**, 054306 (2005); R. S. Iskhakov, S. V. Komogortsev, A. D. Balaev, and L. A. Chekanova, *JETP Lett.* **72**, 304 (2000).